

pubs.acs.org/acsaelm Article

Giant Magnetothermal Conductivity Switching in Semimetallic WSi₂ Single Crystals

Karl G. Koster, Jackson Hise, Joseph P. Heremans, and Joshua E. Goldberger*



Cite This: ACS Appl. Electron. Mater. 2024, 6, 1757–1762

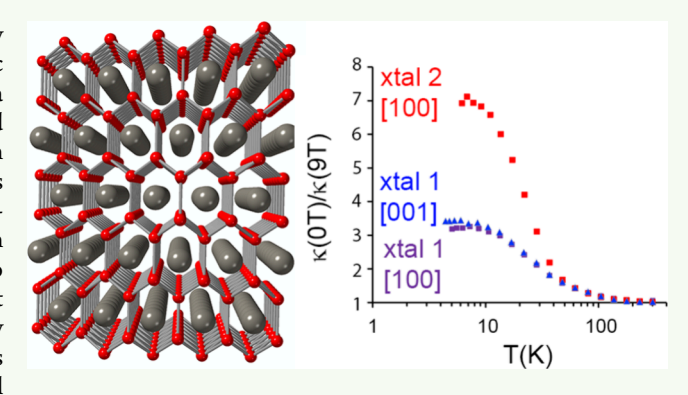


ACCESS |

Metrics & More

Article Recommendations

ABSTRACT: Materials able to rapidly switch between thermally conductive states by external stimuli such as electric or magnetic fields can be used as all-solid-state thermal switches and enable a myriad of applications in heat management, power generation, and cooling. Here, we show that the large magnetoresistance which occurs in highly conducting semimetal α -WSi₂ single crystals leads to dramatically large changes in thermal conductivity at temperatures <100 K. At temperatures <20 K, where electron—phonon scattering is minimized, the thermal conductivity switching ratio between zero field and a 9 T applied field can be >7. We extract the electronic and lattice components of the thermal conductivity and show that the Lorenz number for this material approximates the theoretical value of L_0 . From the heat capacity and thermal



diffusivity, the speed of thermal conductivity switching is estimated to range from 1×10^{-4} s at 5 K to 0.2 s at 100 K for a 5 mm long sample. This work shows that WSi₂, a highly conducting multicarrier semimetal, is a promising thermal switch component for low-temperature applications such as cyclical adiabatic demagnetization cooling, a technology that could replace ³He-based refrigerators.

KEYWORDS: thermal switching, magnetoresistance, thermal conductivity, semimetal, magnetothermal conductivity, Wiedemann–Franz law

■ INTRODUCTION

Compared to the extensive research focused on transistor materials in which the electronic conductance can be actively switched between various states, there has been considerably less effort focused on designing materials, systems, and concepts whose thermal conductance can be actively switched to enable the control of heat flow through a device. All-solid-state heat switches that operate quickly and over large temperature ranges would enable new, durable, wear- and maintenance-free approaches to thermal management. In particular, thermal switches combined with heat accumulators could increase the thermal efficiency of thermodynamic power generation cycles in which the source of heat is transient.

Thermal conductivity switches enable new ways to control the temperature of devices such as batteries⁴ and spacecraft⁵ under varying thermal loads. Heat switches are necessary components for electrocaloric and magnetocaloric solid-state cycles, in which no fluid is circulated but heat must be supplied to or drained from the active material.^{6–8} In these applications, the switches have to function over the temperature range of the cycle and during transient operation such as cooldowns, a requirement that can be difficult to meet with switches based on phase changes in a material. Because the rest of the components throughout the cycle are solid-state with no

moving parts, developing a solid-state heat switch allows for durable, maintenance-free operation of the whole heat engine.

Here, we focus on materials whose thermal conductivities change under applied magnetic fields at temperatures below 10 K. This temperature and field range matches that needed for continuously operating cyclical adiabatic demagnetization refrigerators (ADR's) that operate below 2 K, utilizing the same magnetic field for the magnetocaloric material (a paramagnet like gadolinium gallium garnet, $Gd_3Ga_5O_{12}$) and the thermal switch. ADR's enable electronic loads to reach sub-kelvin temperatures without the use of 3 He, a rare and strategic gas. Continuously operating ADR's are preferred over one-shot methods that operate with helium exchange gas as a switch, as occurs in dilution refrigerators. Heat switches are characterized by their switching ratio, the ratio between the thermal conductance or conductivity of the switch in its "on" and the "off" state, giving a switching ratio (SR) of SR $\equiv \kappa_{on}/\kappa_{off}$.

Received: November 26, 2023 Revised: January 31, 2024 Accepted: February 1, 2024 Published: February 21, 2024





Model calculations⁹ of cyclical ADR's using metallic heat switches that have a SR of the order of 3–10 indicate that a reasonable cooling power of 6–12 μ W/g of gadolinium gallium garnet can be achieved between 2 K and 400 mK, albeit with a low coefficient of performance.

One possible mechanism to actively change the thermal conductivity of a material is by exploiting the electrical magnetoresistance of a material whose primary carriers of thermal conductivity are electrons. In a nonmagnetic metal, the total thermal conductivity (κ_{total}) comes from a summation of the electronic component (κ_{e}) and the phonon contribution to thermal conductivity in which lattice vibrations conduct heat through the material (κ_{l}):

$$\kappa_{\text{total}} = \kappa_{\text{e}} + \kappa_{\text{l}}$$

Each electron that travels through the material carries a charge and an amount of heat, $k_{\rm B}T$ (where $k_{\rm B}$ is the Boltzmann constant and T is the temperature), so that if the scattering mechanisms that limit the mean free path for momentum and energy transport are the same, the Wiedemann–Franz relationship holds between electrical conductivity and thermal conductivity:

$$\kappa_{\rm e} = LT\sigma$$
 (2)

Here, σ is the electrical conductivity, and L is the Lorenz number, which for free electrons is $L_0 = 2.44 \times 10^{-8} \text{ V}^2 \text{ m}^{-2}$. Maximizing the switching ratio between the "on" and the "off" state of a magnetoresistive switch (SR $\equiv \kappa_{on}/\kappa_{off} = \kappa_{total}(0)/\kappa_{off}$ $\kappa_{\text{total}}(B)$) requires very metallic material, where $\kappa_{\text{e}} > \kappa_{\text{l}}$; this is because the lowest value achievable for $\kappa_{total}(B)$ is κ_l . Because the range of κ_1 in most materials lies between ~ 0.1 and 1000 W m⁻¹ K⁻¹ from 1 to 300 K, the Wiedemann–Franz law predicts that the electronic resistivity would have to range from 10⁻⁵ to $10^{-9} \Omega$ m to meet the condition $\kappa_e = \kappa_l$ in the high conductance state. At the same time, the material must have a large magnetoresistance (MR), MR = $[\rho(B) - \rho(0)]/\rho(0)$, where $\rho(B)$ is the electronic resistivity under an applied magnetic field B. These two requirements are mutually counter-indicated in most materials because a high MR comes from a high mobility, and good metals in which κ_e > κ_1 have much lower mobilities than semiconductors because their large Fermi surfaces result in intensive electron-phonon scattering.

Four classes of solutions have been proposed to circumvent this dilemma. The first is to use the giant magnetoresistance in magnetic multilayers such as Co/Cr, in which a cross-plane SR value of ~1.8 has been observed. The second is to use superconducting thermal switches. Superconductors, such as Nb, become normal metals when subject to a magnetic field greater than their critical field, thereby leading to an appreciable reduction in thermal $\kappa_{\rm e}$. Superconducting Sn wires, In switches, and Zn-foil switches have been made and studied, but except at temperatures below 100 mK, their SR's are relatively modest; in all cases, switching can only occur at temperatures below the superconducting transition temperature. The third solution is to use topological Weyl and Dirac semimetals including graphene, 14 PtSn₄, 15 Bi_xSb_{1-x}, 16 and NbP. The condition $\kappa_{\rm e} > \kappa_{\rm l}$ limits the SR in all these solutions, although in PtSn₄ thermal SR > 100 has been observed 15

Nonmagnetic, nonsuperconducting, nontopological semi-metallic materials, like elemental Bi, 18,19 Cd, 20,21 Ga, 20 or W, 22 that have similar carrier densities and mobilities of both holes

and electrons also undergo an appreciable magnetoelectrical resistance, which leads to a significant magnetothermal resistance. This large, nonsaturating magnetoresistance in semimetals comes from electron—hole compensation that gives rise to a mismatch between the Lorentz force and the Hall voltage. Furthermore, when both electrons and holes are present in clean compensated semimetals, the ambipolar thermal conductivity can lead to an increase in L over the free electron value L_0 , which is beneficial for the SR. This increase most commonly occurs in materials in which the electron and hole pockets have the same partial electronic conductivities. Thus, fully evaluating the magnetothermal conductivities in semimetallic materials beyond simple elemental metals is essential to understand and realize their full potential and limitations.

Here we explore the magnetothermal conductivity switching in the compensated semimetal WSi2, a material recently established to exhibit axis-dependent conduction polarity.²² Recent studies have found that at 2 K certain crystals of WSi₂ exhibit a high transverse electronic MR of 4000-8000% at 14 T, where %MR = $100\% \times [\rho(B) - \rho(0)]/\rho(0)$. This large increase in electrical resistivity in the presence of a magnetic field is expected to lead to a large increase in magnetothermal resistance. To investigate the extent to which the thermal conductivity of WSi2 can be manipulated using an applied magnetic field, we evaluated the changes in electrical and thermal conductivities in two different single crystals from 2 to 300 K and 0 to 9 T. The total thermal conductivity can be significantly reduced upon application of a 9 T magnetic field below 20 K, leading to an SR > 7. The SR is larger in the crystal with fewer defects on account of its lower baseline electronic resistivity and larger corresponding magnetoresistance. Negligible differences in the thermal switching ratio or temperature dependence are observed along the [100] or [001] directions. Both MR and SR decrease with increasing temperature, although both crystals retain an SR close to 1.1 at room temperature. We show that the Lorenz number for this material closely matches the free electron value, thereby indicating minimal ambipolar effects that contribute to the thermal conductivity. We also calculate the thermal response time from the specific heat and thermal diffusivity and show that for a 5 mm³ sample switching can occur in less than a second at room temperature and much faster at lower temperatures. Overall, this work shows that ultraclean, compensated semimetallic compounds such as WSi2 show great promise as heat switches.

■ EXPERIMENTAL PROCEDURES

WSi $_2$ crystals were grown using a xenon optical floating zone furnace using a previously described procedure. Crystals were cut into 1 mm \times 1 mm \times 5 mm bars along the [100] and [001] directions using a diamond wire saw to maximize sample resistance, and these samples were lapped and polished using 3 mm diamond grit in oil and a 0.05 mm alumina slurry on a precision lapping and polishing machine to minimize sample geometry variance and contact resistance. Contacts to the surface of the crystal were made using highly thermally and electrically conductive Transene GE-40 gold—epoxy paste with contact areas greater than the contact thicknesses, such that the contacts do not contribute significantly to the thermal and electrical resistance measurements. Transverse magnetoresistance measurements were performed using a four-probe geometry in a Quantum Design 14T PPMS from 2 to 300 K and from 0 to 9 T using the DC resistivity option. Thermal conductivity measurements were per-

formed from 2 to 300 K and from 0 to 9 T using the thermal transport option (TTO) in a Quantum Design 9T PPMS.

RESULTS AND DISCUSSION

 α -WSi₂ crystallizes into a body-centered tetragonal *I4/mmm* crystal structure (Figure 1a). This material has a metallic band

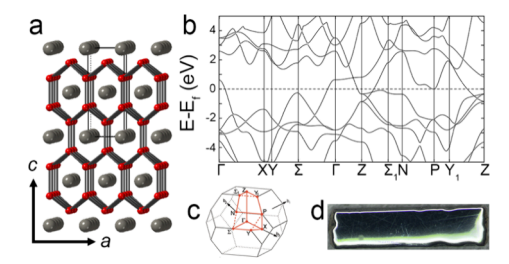


Figure 1. (a) Crystal structure of I4/mmm α -WSi₂. W atoms are shown in gray, and Si atoms are shown in red. The unit cell is drawn in black. (b) Electronic band structure of WSi₂. (c) Brillouin zone for a body-centered tetragonal material with c > a. (d) Photograph of a polished WSi₂ sample (5 mm in length, 1 mm in width and thickness) that was used for magnetoresistance and magnetothermal conductivity measurements.

structure with unique band curvatures that give rise to simultaneous electron and hole conduction along different crystallographic axes (Figure 1b,c).^{4,5} Single crystals of α -WSi₂ previously synthesized using an optical floating zone furnace⁴ were selected to study how the thermal conductivity of WSi2 changes in the presence of an applied magnetic field. These single crystals were confirmed to be phase pure with singlecrystal and powder X-ray diffraction and were oriented along their primary [001] and [100] crystallographic directions using Laue backscattering X-ray diffraction. These rod-shaped crystals were cut into 1 mm × 1 mm × 5 mm bars to maximize sample resistance for electrical measurements, with the crystallographic direction of interest ([100] or [001]) oriented along the length of the bar (Figure 1d). The surfaces of the bars were polished to minimize electrical contact resistances in the measurements and minimize sample geometry variance.

The thermal conductivities of these polished bars of WSia were evaluated from 2 to 300 K in the presence of transversely applied magnetic fields from 0 to 9 T using a steady-state method (Figure 2). At low temperatures (<100 K), the thermal conductivity significantly decreases in the presence of a magnetic field. For crystal 1, the thermal conductivity at 2 K decreased from 37.9 to 11.1 W m⁻¹ K⁻¹ in the [100] direction (Figure 2a) while it decreased from 43.5 to 13.7 W m⁻¹ K⁻¹ in the [001] direction (Figure 2b) when the magnetic field was increased from 0 to 9 T. A switching factor of $\kappa(0 \text{ T})/\kappa(9 \text{ T})$ was determined from the thermal conductivity values measured at 0 and 9 T at each temperature point (Figure 2c). This factor is highest at 2 K, where $SR = \kappa(0 \text{ T})/\kappa(9 \text{ T}) =$ 3.4 along the [100] direction while SR = 3.2 along the [001]direction. For crystal 2 along [100], SR = 7 ± 0.1 at 7 K, and its increase with decreasing temperature is not quite saturated yet. These are remarkable values for a metal. SR approaches unity at 300 K.

To confirm that this reduction in thermal conductivity comes from the large magnetoelectrical resistance observed in WSi $_2$, we measured the electrical resistivity of the two WSi $_2$ crystals from 2 to 300 K when transverse magnetic fields of 0–

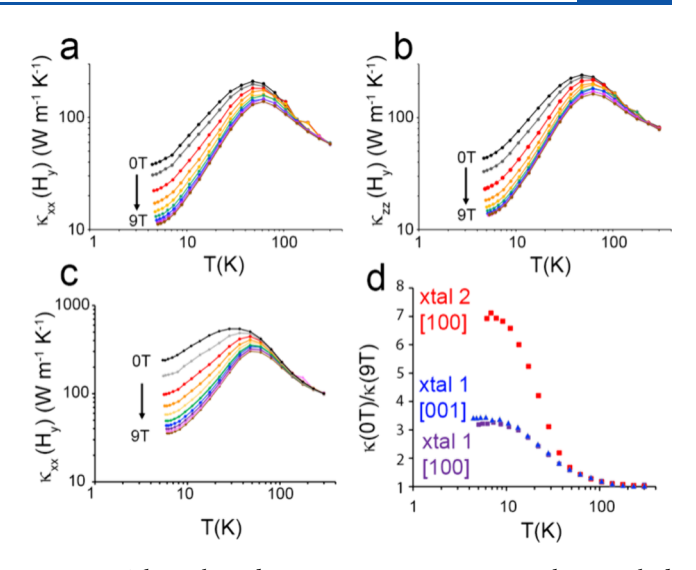


Figure 2. Thermal conductivity versus temperature with an applied transverse magnetic field of 0 to 9 T in 1 T increments for the (a) [100] and (b) [001] directions in crystal 1 and the (c) [100] direction in crystal 2. (d) Thermal conductivity switching factor, calculated as $SR = \kappa(0 \text{ T})/\kappa(9 \text{ T})$.

9T were applied (Figure 3). The residual resistivity values (RRR) from the zero-field measurements (

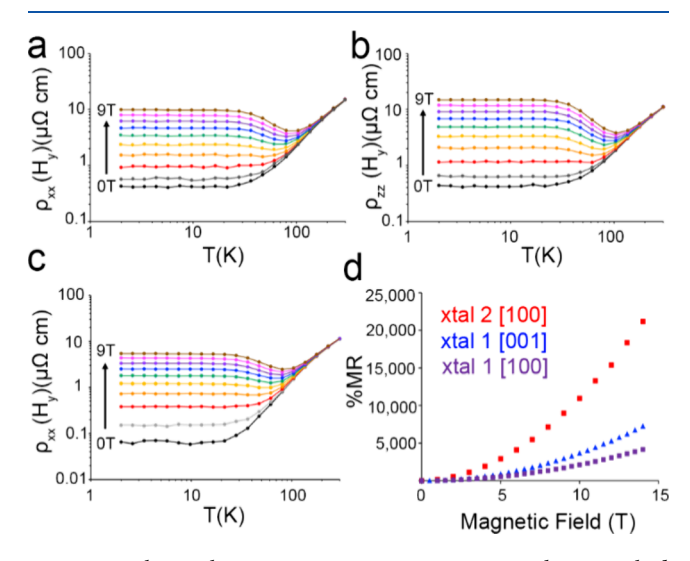


Figure 3. Electrical resistivity versus temperature with an applied transverse magnetic field varying from 0 to 9 at 1 T increments for (a) the [100] and (b) [001] directions in crystal 1 and (c) the [100] direction of crystal 2. (d) %MR measured at 2 K for crystal 1 along the [100] direction (purple), crystal 1 along the [001] direction (blue), and crystal 2 along the [100] direction (red).

RRR = $\frac{\rho(300 \text{ K, 0 T}) - \rho(2 \text{ K, 0 T})}{\rho(2 \text{ K, 0 T})}$) for crystal 1 were 37.6 for the [100] direction (Figure 3a) and 26.9 for the [001] direction (Figure 3b), indicating good crystal quality. Crystal 2 had a much higher RRR of 101, indicative of fewer defects measured along the [100] direction. The presence of fewer defects in crystal 2 was further evidenced by the lower baseline resistivities. The magnetoresistance is maximized at low temperatures in both crystals. The %MR for crystal 1 reached 2200–2400% at 9 T from 2 to 21 K for the [100] direction (Figure 3a) and 3200–3500% at 9 T from 2 to 21 K for the [001] direction (Figure 3b), closely matching previously

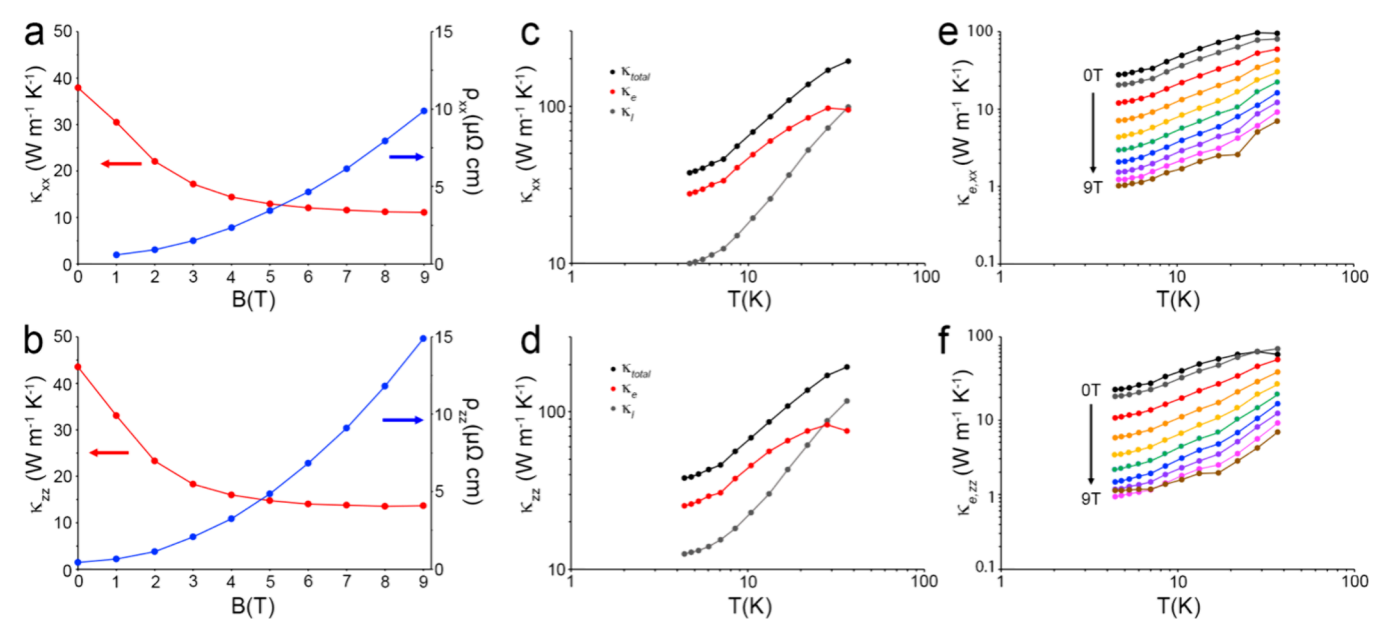


Figure 4. Thermal conductivity (red, left axes) and electrical resistivity (blue, right axes) versus magnetic field at 2 K for the (a) [100] and (b) [001] directions for crystal 1. Plot of κ_{total} (black), κ_{l} (gray), and $\kappa_{\text{e,0T}}$ (red) versus temperature measured along the (c) [100] and (d) [001] directions for crystal 1. κ_{e} plotted versus temperature for magnetic field values of 0–9 T for the (e) [100] and (f) [001] directions for crystal 1.

published values.^{25,26} Crystal 2 had a much larger %MR of ~9000–10000% at 9 T from 2 to 21 K for the [100] direction. Above 21 K, the magnetoresistance effect starts to fall as electron–phonon scattering decreases the mobility of the carriers in the material at higher temperatures, as occurs in nearly all metallic materials.²⁷

The magnetic field-induced reduction in both thermal and electrical conductivities occurs across similar temperature ranges (2-100 K), with the effects being most pronounced at low temperature. Importantly, although the magnetoelectrical resistance in the material increases quadratically with magnetic field and does not saturate, the thermal conductivity decreases asymptotically as the magnetic field is increased. This is because κ_e is nearly eliminated, leaving only $\kappa_{\rm b}$, which remains unchanged in the presence of a magnetic field (Figure 4a,b). The thermal conductivity data do not fully reach saturation at 9 T, but they are expected to do so at higher magnetic fields. To determine the value of κ_1 at each temperature point, the field-dependent thermal conductivity data for each temperature was fitted to the function $\kappa_{\text{total}} = \kappa_{\text{l}} + \frac{\gamma}{1 + \beta^2 R^2}$, in which γ is a linear coefficient, β is a quadratic coefficient representing the magnetoconductivity, and B is the magnetic field. The last term in the equation corresponds to the change in thermal conductivity corresponding to electrical magnetoresistance. The data could only be fit at temperatures up to 36 K. Above this temperature, the much smaller magnetoresistance effect leads to a smaller change in thermal conductivity across all fields, introducing a large uncertainty in the determination of κ_l . Subtracting the fitted value of κ_l from the experimentally determined κ_{total} at 0 T yields a value for κ_e at 0 T, or $\kappa_{e,0T}$. κ_{total} , κ_l , and $\kappa_{e,0T}$ are all plotted together versus temperature up to 36 K in Figure 4c,d. The fact that κ_1 continues to increase across this temperature range indicates that the WSi₂ Debye temperature is above 36 K. κ_e is also plotted from 2 to 36 K and 0 to 9 T in Figure 4e,f, showing how the electronic component of the thermal conductivity decreases at higher field via the magnetoresistance

mechanism. κ_l remains unchanged while κ_e decreases with increasing magnetic field, leading to an overall decrease in κ_{total} when a magnetic field is applied.

Using the $\kappa_{\rm e}$ values that we found by subtracting $\kappa_{\rm l}$ from $\kappa_{\rm total}$, we obtained a value for the Lorenz constant using the Wiedemann–Franz law, $L=\frac{\kappa_{\rm e}}{T\sigma}$. Next, the ratio L/L_0 was calculated at fields from 0 to 9 T and at temperatures from 2 to 36 K to determine if magnetoresistance and magnetothermal conductivity change by the same proportion, which would indicate that this material follows the free-electron Wiedemann–Franz law. The results for both the [100] and the [001] directions are plotted in Figure 5. L/L_0 values for both

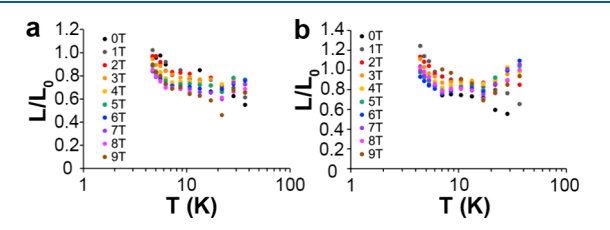


Figure 5. L/L_0 for the (a) [100] and (b) [001] directions under different applied magnetic fields for crystal 1.

crystallographic directions match closely between fields at each given temperature point and are close to 1 (0.6–1.2), indicating that the experimentally observed relationship between magnetothermal conductivity and magnetoelectrical conductivity is relatively proportional and obeys the Wiedemann–Franz law. This proves that the large magnetoresistance in WSi₂ is what gives rise to its accompanying decrease in the thermal conductivity. Furthermore, the fact that L/L_0 is close to 1 and not significantly larger likely reflects the fact that truly ambipolar transport where electrons and holes move together at the same rate under a thermal gradient, rather than as two independent channels of unipolar transport, does not exist in WSi₂. This is because these electrons and holes occupy different regions in the WSi₂ band

structure as well as the anisotropic transport of electron and hole conduction in this tetragonal material with axis-dependent conduction polarity. Holes have a much smaller effective mass along the a/b-axes $|m_{xx,h}^*| = 0.14~m_e$ and $|m_{xx,e}^*| = 2.1~m_e$, while electrons have a much smaller effective mass along the c-axis $|m_{zz,h}^*| = 3.7~m_e$ and $|m_{zz,e}^*| = 0.73~m_e^{.25}$ This indicates that materials that exhibit axis-dependent conduction polarity due to this multicarrier mechanism are unlikely to have large enhancements in L/L_0 that can improve the SR.

To understand the origin in the drop in SR with increasing temperature that starts at 20–30 K (Figure 2d), the mean free paths of both the electrons and holes were derived (Figure 6).

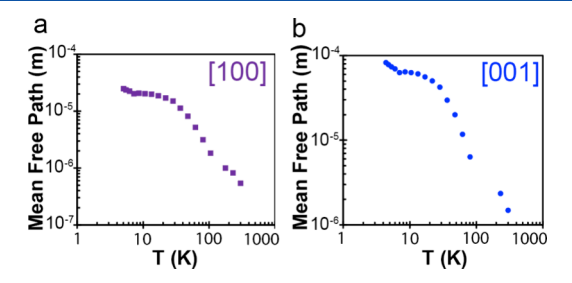


Figure 6. Mean free path of electronic carriers along (a) the [100] and (b) the [001] directions. At low temperatures, the mean free paths change only slightly at low temperatures before dropping below 20–30 K.

First, the constant pressure specific heat was measured at c_p (Figure 7a), which was then converted into constant volume

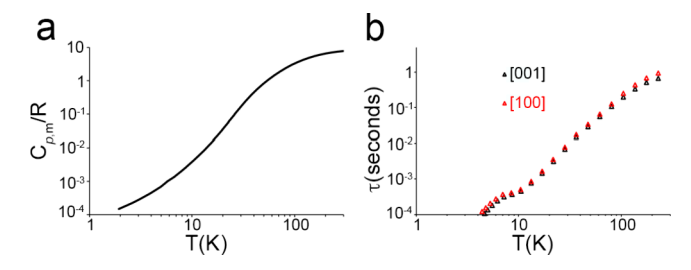


Figure 7. (a) Measured molar heat capacity of crystal 1. (b) Calculated thermal response time for a 5 mm long sample of WSi₂, shown for the [100] (red) and [001] (black) directions.

specific heat, c_V . The electronic portion of the specific was extracted using a Debye T^3 law $(c_V = \gamma T + \alpha T^3)$ where γ and α are constants that correspond to the electronic and phononic contributions, respectively. The electronic contribution to the specific heat, c_e , is given by $c_e = \gamma T$. The mean free path of the electronic carriers, l, is given by $\kappa_e = \frac{1}{3} c_e \nu l$, where ν corresponds to the velocity of carriers. To estimate the carrier velocities along the different directions, we first assumed that electrons dominated κ_e along the [001] direction and holes dominated κ_e along the [100] direction, considering the aforementioned effective mass anisotropies. The velocities of electron and hole carriers were then estimated using the calculated Fermi energies, $E_{\rm F}$, and effective mass tensors of the electron and hole bands, assuming $E_{\rm F,e} = \frac{m_{\rm b,100} \nu^2}{2}$ and $E_{\rm F,h} = \frac{m_{\rm b,100} \nu^2}{2}$. The electron and hole mean free paths (Figure

 $E_{\rm F,h} = \frac{m_{\rm h,100}}{2}$. The electron and hole mean free paths (Figure 6a,b) correspond to ~10 μ m at low temperatures and remain almost constant until 20–30 K, until they decrease proportionally with temperature. This behavior is indicative of defect

scattering at low temperatures and the emergence of acoustic phonon scattering occurring above 20–30 K, which is the temperature at which the SR starts to significantly decrease. This indicates that increasing the temperature at which acoustic phonon scattering starts to dominate would lead to a higher temperature before SR dropoff occurs.

A functional thermal switch should be capable of rapidly switching between the conductive and nonconductive states. This rate is limited by the thermal diffusivity of the material (given in m²/s), with diffusivity equal to the thermal conductivity divided by the specific heat capacity: $\alpha = \kappa/$ (ρc_p) , in which α is the diffusivity, c_p is the specific heat capacity in J/(kg K), and ρ is the material density in kg/m³. The experimentally measured molar heat capacity $(c_{v,m})$ is plotted in Figure 7a and, along with the thermal conductivity data plotted in Figure 2, can be used to determine the thermal diffusivity of the material. Then, a thermal response time for a sample of a certain size is given by $\tau = l^2/\alpha$, in which τ is the time constant and l is the sample length. This value of τ is given for a 5 mm long sample of WSi₂ in Figure 7b. τ values are nearly isotropic along both primary crystallographic directions, ranging from 1×10^{-4} s at 2 K to 0.8–1.1 s at 300 K. Practically, this means that the thermal switching speed will ultimately be dictated by the speed in which a magnetic field can be applied to the material, which is much faster than our current measurement setup.

CONCLUSIONS

In total, we have shown that a single-crystal, compound semimetal, WSi2, can have giant changes in thermal conductivity upon application of a magnetic field at low temperature. Specifically, a large 9000-10000% magnetoresistance in WSi₂ at low temperatures of 2-21 K and fields of 0-9 T can be attributed to the electron-hole compensation in this two-carrier material and gives rise to an accompanying 7fold decrease in the material's thermal conductivity, which closely follows the Wiedemann-Franz law. Furthermore, a WSi2 crystal with a larger relative resistivity ratio has a larger SR, indicating that further minimization of defects during crystal growth will provide opportunities to enhance the magnitude of thermal switching. The appreciable change in the thermal conductivity in the presence of a magnetic field, along with the material's ability to rapidly switch between thermally conductive and less conductive states, makes WSi2 a promising material system for thermal switching applications at low temperatures.

AUTHOR INFORMATION

Corresponding Author

Joshua E. Goldberger — Department of Chemistry and Biochemistry, The Ohio State University, Columbus, Ohio 43210, United States; orcid.org/0000-0003-4284-604X; Email: goldberger.4@osu.edu

Authors

Karl G. Koster – Department of Chemistry and Biochemistry, The Ohio State University, Columbus, Ohio 43210, United States

Jackson Hise – Department of Mechanical and Aerospace Engineering, The Ohio State University, Columbus, Ohio 43210, United States Joseph P. Heremans – Department of Mechanical and Aerospace Engineering and Department of Physics, The Ohio State University, Columbus, Ohio 43210, United States

Complete contact information is available at: https://pubs.acs.org/10.1021/acsaelm.3c01662

Notes

The authors declare no competing financial interest.

ACKNOWLEDGMENTS

This work was primarily supported by the ONR MURI "Extraordinary electronic switching of thermal transport", Grant N00014-21-1-2377, for J.E.G., K.G.K., and J.P.H. J.H. was supported by NSF CBET Grant "EAGER: CRYO: Development of a sub-kelvin refrigerator using magnetic field activated solid-state thermal switches based on thermal chiral anomaly", Grant CBET 2232811. The material used in this work was supported by the NSF-MIP Platform for the Accelerated Realization, Analysis, and Discovery of Interface Materials (PARADIM) under Cooperative Agreement No. DMR-2039380. Partial funding for shared facilities used in this research was provided by the Center for Emergent Materials: an NSF MRSEC under Award DMR-2011876. The authors acknowledge Lucas Pressley and Mojammel Khan at the NSF PARADIM facility for helping to grow large single crystals of WSi₂.

REFERENCES

- (1) Wehmeyer, G.; Yabuki, T.; Monachon, C.; Wu, J.; Dames, C. Thermal Diodes, Regulators, and Switches: Physical Mechanisms and Potential Applications. *Appl. Phys. Rev.* **2017**, *4*, 041304.
- (2) Liu, C. H.; Chen, Z. H.; Wu, C.; Qi, J.; Hao, M. L.; Lu, P.; Chen, Y. F. Large Thermal Conductivity Switching in Ferroelectrics by Electric Field-Triggered Crystal Symmetry Engineering. ACS Appl. Mater. Interfaces 2022, 14 (41), 46716–46725.
- (3) Qian, X.; Zhou, J. W.; Chen, G. Phonon-Engineered Extreme Thermal Conductivity Materials. *Nat. Mater.* **2021**, 20 (9), 1188–1202.
- (4) Du, T.; Xiong, Z.; Delgado, L.; Liao, W.; Peoples, J.; Kantharaj, R.; Chowdhury, P. R.; Marconnet, A.; Ruan, X. Wide Range Continuously Tunable and Fast Thermal Switching Based on Compressible Graphene Composite Foams. *Nat. Commun.* **2021**, 12, 4915.
- (5) Hengeveld, D. W.; Mathison, M. M.; Braun, J. E.; Groll, E. A.; Williams, A. D. Review of Modern Spacecraft Thermal Control Technologies. *HVAC&R Res.* **2010**, *16* (2), 189–220.
- (6) Klinar, K.; Vozel, K.; Swoboda, T.; Sojer, T.; Rojo, M. M.; Kitanovski, A. Ferrofluidic Thermal Switch in a Magnetocaloric Device. *iScience* **2022**, 25 (2), No. 103779.
- (7) Klinar, K.; Kitanovski, A. Thermal Control Elements for Caloric Energy Conversion. *Renewable Sustainable Energy Rev.* **2020**, *118*, 109571.
- (8) Silva, D. J.; Bordalo, B. D.; Pereira, A. M.; Ventura, J.; Araujo, J. P. Solid State Magnetic Refrigerator. *Appl. Energy* **2012**, *93*, 570–574.
- (9) Shirron, P. Optimization Strategies for Single-Stage, Multi-Stage and Continuous Adrs. *Cryogenics* **2014**, *62*, 140–149.
- (10) Franz, R.; Wiedemann, G. Ueber Die Wärme-Leitungsfähigkeit Der Metalle. Ann. Phys. (Berlin, Ger.) 1853, 165, 497-531.
- (11) Kimling, J.; Wilson, R. B.; Rott, K.; Kimling, J.; Reiss, G.; Cahill, D. G. Spin-Dependent Thermal Transport Perpendicular to the Planes of Co/Cu Multilayers. *Phys. Rev. B: Condens. Matter Mater. Phys.* **2015**, *91* (14), No. 144405.
- (12) Wasim, S. M.; Zebouni, N. H. Thermal Conductivity of Superconducting Niobium. *Phys. Rev.* **1969**, *187* (2), 539.
- (13) Schuberth, E. Superconducting Heat Switch of Simple Design. Rev. Sci. Eng. 1984, 55 (9), 1486–1488.

- (14) Crossno, J.; Shi, J. K.; Wang, K.; Liu, X.; Harzheim, A.; Lucas, A.; Sachdev, S.; Kim, P.; Taniguchi, T.; Watanabe, K.; Ohki, T. A.; Fong, K. C. Observation of the Dirac Fluid and the Breakdown of the Wiedemann-Franz Law in Graphene. *Science* **2016**, *351* (6277), 1058–1061.
- (15) Fu, C. G.; Guin, S. N.; Scaffidi, T.; Sun, Y.; Saha, R.; Watzman, S. J.; Srivastava, A. K.; Li, G. W.; Schnelle, W.; Parkin, S. S. P.; Felser, C.; Gooth, J. Largely Suppressed Magneto-Thermal Conductivity and Enhanced Magneto-Thermoelectric Properties in PtSn₄. *Research* **2020**, 2020, No. 4643507.
- (16) Vu, D.; Zhang, W. J.; Sahin, C.; Flatte, M. E.; Trivedi, N.; Heremans, J. P. Thermal Chiral Anomaly in the Magnetic-Field-Induced Ideal Weyl Phase of Bi_{1-x}Sb_x. *Nat. Mater.* **2021**, *20* (11), 1525–1531.
- (17) Gooth, J.; Niemann, A. C.; Meng, T.; Grushin, A. G.; Landsteiner, K.; Gotsmann, B.; Menges, F.; Schmidt, M.; Shekhar, C.; Suß, V.; Hühne, R.; Rellinghaus, B.; Felser, C.; Yan, B.; Nielsch, K. Experimental Signatures of the Mixed Axial-Gravitational Anomaly in the Weyl Semimetal NbP. *Nature* **2017**, *547* (7663), 324–327.
- (18) Alers, P. B.; Webber, R. T. The Magnetoresistance of Bismuth Crystals at Low Temperatures. *Phys. Rev.* **1953**, *91* (5), 1060–1065.
- (19) Uher, C.; Goldsmid, H. J. Separation of the Electronic and Lattice Thermal Conductivities in Bismuth Crystals. *Phys. Status Solidi B* **1974**, *65*, 765–772.
- (20) Mendelssohn, K. A. G.; Rosenberg, H. M. The Thermal Conductivity of Metals in High Magnetic Fields at Low Temperatures. *Proc. R. Soc. London* **1953**, *A218*, 190–205.
- (21) Laudy, J.; Knol, A. A Cadmium Heat Switch. Cryogenics 1966, 6, 370.
- (22) Batdalov, A.; Red'ko, N. Lattice and Electronic Thermal Conductivities of Pure Tungsten at Low Temperatures. *Sov. Phys. Solid State* **1980**, 22, 664–666.
- (23) Zhang, S.; Wu, Q.; Liu, Y.; Yazyev, O. V. Magnetoresistance from Fermi Surface Topology. *Phys. Rev. B* **2019**, *99*, 35142.
- (24) Zarenia, M.; Principi, A.; Vignale, G. Thermal Transport in Compensated Semimetals: Effect of Electron-Electron Scattering on Lorenz Ratio. *Phys. Rev. B* **2020**, *102* (21), No. 214304.
- (25) Koster, K. G.; Deng, Z.; Moore, C. E.; Heremans, J. P.; Windl, W.; Goldberger, J. E. Axis-Dependent Conduction Polarity in WSi₂ Single Crystals. *Chem. Mater.* **2023**, *35* (11), 4228–4234.
- (26) Mondal, R.; Sasmal, S.; Kulkarni, R.; Maurya, A.; Nakamura, A.; Aoki, D.; Harima, H.; Thamizhavel, A. Extremely Large Magnetoresistance, Anisotropic Hall Effect, and Fermi Surface Topology in Single-Crystalline WSi₂. *Phys. Rev. B* **2020**, *102*, No. 115158.
- (27) Putley, E. H. The Hall Effect and Related Phenomena; Butterworth & Co. Limited: 1960.